

Moving Transversal Hot Zones in Adiabatic, Shallow Packed-Bed Reactors

Ganesh A Viswanathan and Dan Luss

Dept. of Chemical Engineering, University of Houston, Houston, TX 77204

DOI 10.1002/aic.10647

Published online September 28, 2005 in Wiley InterScience (www.interscience.wiley.com).

*Transversal hot zones have been observed in industrial and laboratory packed-bed reactors. Yet, previous modeling attempts failed to predict them without making the unrealistic assumption that the transversal heat dispersion exceeds that of the reactants. It is shown that the formation of transversal hot zones in a uniformly active catalytic reactor is strongly dependent on the reaction kinetics. For example, transversal spatio-temporal concentration and temperature patterns can be predicted to form in a shallow adiabatic packed-bed reactor using realistic parameters for a catalytic reaction, the rate of which may oscillate under constant ambient conditions. Various experimentally tested rate expressions, such as those describing the oxidation of CO, exhibit this feature. A large number of different types of stable, transversal patterns may form for a sufficiently large reactor diameter, most of which do not exhibit azimuthal symmetry. Surprisingly, the time-averaged effluent reactant concentration and the period of the different spatiotemporal patterns are rather similar and close to those obtained under a uniform oscillating state. A systematic procedure is presented for finding the initial conditions leading to formation of the different patterns. Numerical simulations show that, because of their homoclinic features, the spatiotemporal patterns have a long period (order of hours), in agreement with various reported laboratory experiments. © 2005 American Institute of Chemical Engineers *AIChE J*, 52: 705–717, 2006*

Keywords: packed-bed reactors, transversal hot zones, transversal concentration patterns, oscillatory kinetics, homoclinic motion

Introduction

A uniform temperature is usually expected to exist in the cross section of an adiabatic packed-bed reactor. However, formation of transversal (perpendicular to the flow direction) local hot zones has been reported to occur in various adiabatic industrial and laboratory reactors. Boreskov et al.¹ and Matros² observed several, azimuthally nonsymmetric hot zones at the exit of a packed-bed reactor during the partial oxidation of isobutyl alcohol. Barkelew and Gambhir³ reported the formation of clinkers—small lumps of molten catalyst—during hydrosulfurization in trickle-bed reactors. Wicke and Onken^{4,5}

observed a nonuniformity of transversal temperature in a laboratory packed-bed reactor during the oxidation of CO. Infrared imaging revealed temperature pattern formation in various laboratory reactors including the exterior surface of a radial flow reactor^{6,7} and the top of shallow packed-bed reactors.^{8–11} Sundarram et al.¹² indicated that global coupling between the effluents and the top of the reactor affected these temperature patterns.

Local hot zones may decrease the yield of the desired products and deactivate the catalyst. In addition, they may initiate undesired highly exothermic reactions that have a negligible rate under uniform temperature operation, leading to a runaway. It is very difficult to detect small transversal hot regions in large commercial reactors. They can create severe safety hazards when present next to the reactor walls by decreasing the metal strength, which in turn may cause a crack in the

Correspondence concerning this article should be addressed to D. Luss at dluss@uh.edu.

reactor wall and the subsequent release of reactants and products may lead to an explosion. Several explosions of trickle-bed reactors have been attributed to this situation. Clearly, understanding and the ability to predict the conditions leading to evolution of local hot zones are of paramount industrial importance because it is a prerequisite for developing operation and control procedures that circumvent their formation.

Matros² showed that transversal hot spots may form as a result of nonuniform packing of the reactor. Obviously, non-uniformly active reactor could generate transversal hot zones. Jaffe¹³ showed that an internal obstruction may lead to hot spot formation during the hydrogenation process. Balakotaiah's research group¹⁴⁻¹⁷ showed that spatiotemporal temperature patterns may evolve as a result of hydrodynamic instabilities in a down-flow packed-bed reactor. However, this occurred for flow rates much lower than those in commercial reactors. Similarly, Benneker et al.¹⁸ indicated that hydrodynamic instability may generate hot and cold spots under certain conditions in an adiabatic packed-bed reactor. Middy et al.¹⁹ showed that temperature and concentration patterns may form on the surface of a catalyst as a consequence of global coupling between the surface and the mixed reactants in a continuous stirred tank reactor (CSTR) whose temperature is kept constant. Nekhamkina et al.²⁰ showed that during the oxidation of CO various temperature patterns may form on a catalytic fiber cloth as a result of the global coupling between the catalyst and the mixed reactants in a CSTR, kept at a constant temperature.

Previous attempts to predict temperature pattern formation by a traditional adiabatic packed-bed reactor model required use of unrealistic parameter values. Schmitz and Tsotsis²¹ found that the stationary patterns formed in a chain of interacting catalyst pellets only when the rate of species exchange exceeded that of heat exchange. However, the heat exchange is greater than that of the species. Balakotaiah et al.²² found that temperature patterns may form in an adiabatic packed-bed reactor used to conduct a bimolecular reaction (with Langmuir-Hinshelwood kinetics), if the rate of transversal heat dispersion is lower than that of the species. However, Yakhin and Menzinger²³ indicated that the dispersion of heat is greater than that of the species in packed-bed reactors. Viswanathan et al.²⁴ proved that a two-variable (temperature and reactant concentration) pseudo-homogeneous model of a (shallow) adiabatic packed-bed reactor cannot predict the formation of a stable, stationary temperature pattern, if it accounts for the fact that the transversal dispersion of heat is greater than that of the reactants. This stability analysis was conducted for reactions whose rate depends only on the surface concentration of a limiting reactant and temperature. In this study, we use a more detailed rate expression that depends—in addition to the concentration of the limiting reactant and temperature—on the adsorbed concentration of a nonlimiting reactant.

Experiments by Ertl's research group revealed that surface concentration patterns may evolve under isothermal conditions on catalytic surfaces exposed to constant reactant concentration.²⁵ Several theoretical models can predict such concentration pattern formation under isothermal conditions. These models use kinetic expressions that can lead to isothermal rate oscillations. The mechanisms that lead to these oscillatory rate expressions include such phenomena as reaction-induced surface restructuring,^{26,27} impact of subsurface reactant adsorption,²⁸⁻³² reversible adsorption desorption of a poison,³³⁻³⁵ and

cluster formation.³⁶ These rate expressions have successfully predicted experimental observations. Depending on the initial conditions, these models usually lead to evolution of either a uniform oscillatory state or one with a spatiotemporal concentration pattern. So far, there is no information on the total number of the possible stable patterns that may form or of the initial conditions that lead to their formation.

The above experiments and models and the spatiotemporal nature of most laboratory observations motivated our study. The first and main goal is to demonstrate the possibility of predicting transversal temperature patterns by a model with realistic parameters for a reaction, such as CO oxidation, that can exhibit isothermal rate oscillations. The second goal is to develop a systematic procedure for predicting the possible different stable temperature patterns and the initial conditions that lead to their formation. The third goal is to determine the impact of the difference between the various patterned states on the time-averaged effluent reactant concentration and period of oscillations.

Mathematical Model

We investigate pattern formation using a pseudo-homogeneous model of a uniformly active adiabatic packed-bed reactor, in which a single catalytic reaction,



occurs, with a large excess of *B* in the feed. The model accounts for mass transfer resistance between the gaseous and adsorbed reactant concentration and for the heat dispersion being greater than that of the species. We assume that all the physical properties are independent of the temperature and species concentrations. We account for the effective thermal conductivity by the Vortmeyer and Schaefer³⁷ relation

$$\bar{\lambda} = \bar{\lambda}_{sg} + (1 - \varepsilon)\bar{\lambda}_s \quad (2)$$

where $\bar{\lambda}_{sg} = [v^2(\rho C_p)_g^2/(ha_c)]$ accounts for the heat transfer between the gas and catalyst pellets. The concentration of the gaseous reactant *A* and the dimensionless temperature satisfy the following equations:

$$\frac{\partial c}{\partial \tau} = \frac{1}{\text{Pe}_\perp^m} \nabla_\perp^2 c + \frac{1}{\text{Pe}_a^m} \frac{\partial^2 c}{\partial \eta^2} - \frac{\partial c}{\partial \eta} - N_c \mathbb{G}_1(x, y, c, \theta) \quad (3)$$

$$\frac{\partial \theta}{\partial \tau} = \frac{1}{\text{Le}} \left[\frac{1}{\text{Pe}_\perp^h} \nabla_\perp^2 \theta + \frac{1}{\text{Pe}_a^h} \frac{\partial^2 \theta}{\partial \eta^2} - \frac{\partial \theta}{\partial \eta} + \beta N_c \mathbb{R}(x, y, \theta) \right] \quad (4)$$

where *x* and *y* are the fractional surface coverage of species *A* and *B* and $\mathbb{G}_1(x, y, c, \theta)$ and $\mathbb{R}(x, y, \theta)$ are the net rate of *A* adsorption and the reaction rate per unit surface area of the catalyst, respectively. ∇_\perp^2 is the Laplacian in ξ and ϕ coordinates.

The dimensionless variables and parameters are

$$c = C_A/C_{A,in} \quad \theta = (T - T_{in})/T \quad \tau = t v/L$$

$$\eta = z/L \quad \xi = r/R \quad N_c = a_v M/C_{A,in}$$

$$\begin{aligned} \text{Pe}_a^h &= \frac{vL}{\bar{\lambda}_a/(\rho C_p)_g} & \text{Pe}_a^m &= vL/D_a & \beta &= \frac{(-\Delta H)C_{in}}{(\rho C_p)_g T_{in}} & \frac{dy}{d\tau} &= \mathbb{G}_2(x, y, \theta) - \mathbb{R}(x, y, \theta) \end{aligned} \quad (11)$$

$$\begin{aligned} \text{Pe}_\perp^h &= \frac{vR^2}{L\bar{\lambda}_\perp/(\rho C_p)_g} & \text{Pe}_\perp^m &= vR^2/(LD_\perp) & & & & \text{where} \end{aligned}$$

$$\text{Le} = \varepsilon + (1 - \varepsilon) \frac{(\rho C_p)_s}{(\rho C_p)_g} \quad (5) \quad \mathbb{G}_1(x, y, c, \theta) = \text{Da}_1 \exp\left(\frac{\gamma_1 \theta}{1 + \theta}\right)$$

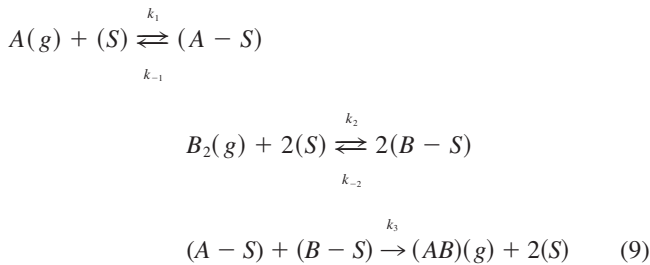
where M is the surface adsorption capacity. The transversal heat and species dispersion coefficients ($\bar{\lambda}_\perp$ and D_\perp) differ from those in the axial direction ($\bar{\lambda}_a$ and D_a). The corresponding boundary conditions are

$$\frac{1}{\text{Pe}_a^h} \frac{\partial \theta}{\partial \eta} = \theta \quad \frac{1}{\text{Pe}_a^m} \frac{\partial c}{\partial \eta} = c - 1 \quad \eta = 0 \quad (6)$$

$$\frac{\partial \theta}{\partial \eta} = \frac{\partial c}{\partial \eta} = 0 \quad \eta = 1 \quad (7)$$

$$\frac{\partial \theta}{\partial \xi} = \frac{\partial c}{\partial \xi} = 0 \quad \xi = 1 \quad (8)$$

We consider here a reaction whose rate may exhibit isothermal rate oscillations. Such behavior has been observed for various reactions, CO oxidation being the one most extensively investigated. The investigative team of Ertl has clearly demonstrated that such oscillations may be encountered under isothermal conditions.²⁵⁻²⁷ Isothermal rate oscillations can be predicted by kinetic models in which the reaction rate depends, in addition to the adsorbed surface reactant concentration, on an additional variable, such as the temporal state of the surface,³¹ subsurface reactant concentration^{32,38} or fractional surface coverage.^{28,30} Here we use a kinetic model that contains a minimal number of parameters and assumes that the reaction proceeds by the Langmuir–Hinshelwood mechanism, as follows:



Following Slinko,²⁸⁻³⁰ we assume that the reaction rate constant k_3 depends on the fractional surface coverage of species B , y . We consider a case in which the product immediately desorbs from the surface after being formed. The fractional surface coverage of the adsorbed species satisfy the equations

$$\frac{dx}{d\tau} = \mathbb{G}_1(x, y, c, \theta) - \mathbb{R}(x, y, \theta) \quad (10)$$

$$c(1 - x - y) - \text{Da}_{-1} \exp\left(\frac{\gamma_{-1} \theta}{1 + \theta}\right) x \quad (12)$$

$$\mathbb{R}(x, y, \theta) = \text{Da} \exp\left(\frac{\gamma_3 \theta}{1 + \theta}\right) xy \exp(-\mu y) \quad (13)$$

$$\begin{aligned} \mathbb{G}_2(x, y, \theta) &= \text{Da}_2 \exp\left(\frac{\gamma_2 \theta}{1 + \theta}\right) (1 - x - y)^2 \\ &\quad - \text{Da}_{-2} \exp\left(\frac{\gamma_{-2} \theta}{1 + \theta}\right) y^2 \end{aligned} \quad (14)$$

$$\begin{aligned} \text{Da}_1 &= \frac{k_1(T_{in})C_{A,in}L}{v} & \text{Da}_{-1} &= \frac{k_{-1}(T_{in})L}{v} \\ \text{Da}_2 &= \frac{2k_2(T_{in})C_{B,in}L}{v} & \text{Da}_{-2} &= \frac{2k_{-2}(T_{in})L}{v} \\ \text{Da} &= \frac{k_3(T_{in})L}{v} & \gamma_i &= E_i/(\bar{R}T_{in}) \\ k_i(T_{in}) &= k_{i0} \exp(-\gamma_i) & \forall i &= 1, -1, 2, -2, 3 \end{aligned} \quad (15)$$

Our goal is to predict the conditions under which transversally nonuniform states may occur and to gain insight into their stability and dynamics. Unfortunately, both the analysis and dynamic simulations of the full model are rather demanding and difficult to present in a paper. Thus, to simplify the model analysis and presentation we consider here a reduced version of the full model: that of a shallow reactor ($\mathbb{S}\mathbb{R}$), obtained by a Liapunov–Schmidt reduction³⁹ of the full model. A similar simplifying approach was previously used by Balakotaiah et al.⁴⁰ and Viswanathan et al.²⁴ Details of the reduction procedure are described by Viswanathan.⁴¹

The shallow reactor model consists of Eqs. 10 and 11 and

$$\frac{\partial \theta}{\partial \tau} = \frac{1}{\text{Le}} \left[\frac{1}{\text{Pe}_\perp^h} \nabla_\perp^2 \theta - \theta + \beta N_c \text{Da} \exp\left(\frac{\gamma_3 \theta}{1 + \theta}\right) xy \exp(-\mu y) \right] \quad (16)$$

$$\begin{aligned} \frac{\partial c}{\partial \tau} &= \frac{1}{\text{Pe}_\perp^m} \nabla_\perp^2 c + (1 - c) - N_c \left[\text{Da}_1 \exp\left(\frac{\gamma_1 \theta}{1 + \theta}\right) c(1 - x - y) \right. \\ &\quad \left. - \text{Da}_{-1} \exp\left(\frac{\gamma_{-1} \theta}{1 + \theta}\right) x \right] \end{aligned} \quad (17)$$

where we denote by θ and c the spatial (axial) averaged quantities in the shallow reactor model, that is,

$$\theta = \int_0^1 \theta d\eta \quad c = \int_0^1 c d\eta \quad (18)$$

The corresponding boundary conditions are

$$\frac{\partial \theta}{\partial \xi} = \frac{\partial c}{\partial \xi} = 0 \quad \xi = 1 \quad (19)$$

The numerical solution was obtained by discretizing the model using a second-order central difference scheme. To circumvent the singularity at the center ($\xi = 0$), the grid points were placed at the radial positions $\xi_j = (2j - 1)/(2N - 1) \forall j = 1, N$.⁴² The discretized model is similar to a cell model in a circular cross section, with the diffusion terms (in the continuous model) mimicked by exchange coefficients among the cells. The dynamic simulations were conducted using a linear implicit extrapolator (LIMEX).^{43,44} The one dimensional calculations were conducted using the LAPACK option. The two-dimensional calculations were conducted using a sparse iterative linear solver (GMRES/BiCGSTAB). The sparse iterative solver in the linear step usually converged in two to three iterations. Steady-state calculations were performed using Newton iteration.

Procedure of Finding Spatiotemporal States

Our study is the first to show that transversal hot zones may form in a uniformly active, adiabatic shallow packed-bed reactor in which the transversal heat dispersion exceeds that of the reactants. To find these states we first construct the boundary of the parameter region in which these hot zones can form. We then apply initial conditions that lead to their evolution.

The oscillatory kinetic model we use can lead to stable, homogeneous oscillations within a bounded range of a bifurcation parameter. The branch of these solutions emanates from two Hopf bifurcation points, determined by a linear stability analysis of the uniform solutions.

A stable uniform state may become unstable to inhomogeneous transverse perturbations

$$\mathbf{u}_{mn} = \mathbf{u}_{ss} + A \mathbf{J}_m(\mu_{mn} \xi) e^{im\phi} \quad (20)$$

where J_m is the Bessel function of first kind. (J_m is real in our problem because of the no-flux boundary conditions.⁴⁵) This stability transition occurs at the neutral stability point, leading to evolution of nonuniform states. The neutral stability curve is the locus of neutral stability points in a two-parameter plane. At a neutral stability point

$$\mathbb{F}(\mathbf{u}_{ss}, Da) = 0 \quad (21)$$

$$[\mathbb{D}_u \mathbb{F}|_{\mathbf{u}_{ss}} - \mathbb{P}] \cdot (\boldsymbol{\omega}_r \pm i \boldsymbol{\omega}_i) = \pm i \sigma (\boldsymbol{\omega}_r \pm i \boldsymbol{\omega}_i) \quad (22)$$

where \mathbb{F} represents the steady-state model equations, $\mathbb{D}_u \mathbb{F}|_{\mathbf{u}_{ss}}$ is the first Fréchet derivative of \mathbb{F} with respect to \mathbf{u} evaluated at the steady state \mathbf{u}_{ss} , \mathbb{P} is the transverse perturbation matrix, σ is the coefficient of the imaginary eigenvalue, and $\boldsymbol{\omega} = \boldsymbol{\omega}_r \pm i \boldsymbol{\omega}_i$ are the corresponding complex eigenvectors. Thus, the

neutral stability point is obtained by solving Eq. 21 simultaneously with

$$[\mathbb{D}_u \mathbb{F}|_{\mathbf{u}_{ss}} - \mathbb{P}] \cdot \boldsymbol{\omega}_r + \sigma \boldsymbol{\omega}_i = 0 \quad (23)$$

$$[\mathbb{D}_u \mathbb{F}|_{\mathbf{u}_{ss}} - \mathbb{P}] \cdot \boldsymbol{\omega}_i - \sigma \boldsymbol{\omega}_r = 0 \quad (24)$$

$$\|\boldsymbol{\omega}_r\| + \|\boldsymbol{\omega}_i\| - 1 = 0 \quad (25)$$

$$\boldsymbol{\omega}_r \cdot \boldsymbol{\omega}_i = 0 \quad (26)$$

The base state (\mathbf{u}_{ss}) used in the linear stability analysis of the uniform state and of the neutral stability is the same because of the no-flux boundary conditions. At very large values of R/d_p , the transversal Pe is very large and the contribution of the transversal dispersion becomes negligible. Thus, the neutral stability points at very large R/d_p asymptotically approach the bifurcation parameter at which the uniform state has a Hopf bifurcation point. Starting at a neutral stability point at very large R/d_p , a pseudo-arc length continuation with respect to R/d_p is used to compute the oscillatory neutral stability curve for a specific transversal inhomogeneous perturbation (m and n values in Eq. 20) in the R/d_p vs. the bifurcation variable plane. This curve bounds a region in which nonuniform state solutions exist.

The nonuniform states are stable only within a certain region of attraction, that is, they are attained only from certain sets of initial conditions. To find a specific inhomogeneous state, we choose R/d_p and a Da value slightly above the neutral stability curve for the specified m and n values. We then conduct dynamic simulations using as the initial condition

$$\mathbf{u} = \mathbf{u}_{ss} + A \mathbf{u}_{mn}(\mu_{mn} \xi) e^{im\phi} \quad (27)$$

where the coefficient A was usually taken to be unity. When the initial condition did not lead to the desired state, another value of A in [0.1, 1.0] was used. After a nonuniform state was obtained close to a neutral stability curve, a sequence of dynamic simulations for slightly perturbed parameters can be used to find this state at other sets of parameters.

We shall illustrate this procedure by first finding states exhibiting different spatiotemporal concentration patterns in an isothermal shallow bed. We show this case first because it enables analytical determination of the Hopf bifurcation points. Next we apply the procedure to predict spatiotemporal temperature patterns in a shallow adiabatic packed-bed reactor.

In all the simulations we used the activation energy data suggested by Slinko and Jaeger⁴⁶ for the adsorption-desorption steps. The adsorption-desorption Da values were based on those used by Ivanov et al.³⁰ The kinetic and other model parameters used in all the simulations are

$$\begin{aligned} \gamma_1 &= 0 & \gamma_{-1} &= 2.04 & \gamma_2 &= 1.02 & \gamma_{-2} &= 34.7 \\ Da_1 &= 4.5 \times 10^{-4} & L/d_p &= 1.0 & Da_{-1} &= 1.56 \times 10^{-5} \\ Da_2 &= 7.29 \times 10^{-4} & Da_{-2} &= 4.25 \times 10^{-7} & \mu &= 15 \\ Le &= 1000 & N_c &= 2000 & \gamma_3 &= 14.3 & \beta &= 0.3 \end{aligned}$$

$$\text{Pe}_\perp^m = 5.0(R/d_p)^2 \quad \text{Pe}_\perp^h = 1.0(R/d_p)^2 \quad (28)$$

Note that the transversal dispersion of heat is fivefold larger than that of the reactants, that is,

$$\text{Pe}_\perp^m = 5\text{Pe}_\perp^h \quad (29)$$

Spatiotemporal Concentration Patterns in an Isothermal Shallow Reactor

We consider the spatiotemporal dimensionless concentration patterns forming in an isothermal shallow reactor, that is, $\beta = 0$ and $\theta = 0$. In the isothermal case, the four-variable $\mathbb{S}\mathbb{R}$ model (Eqs. 10, 11, 16, and 17) is reduced to a three-variable model, that is, Eqs. 10, 11, and 17 with $\theta = 0$. At steady state,

$$x = \frac{\text{Da}_1 c(1-y)}{\text{Da}_1 c + \text{Da}_{-1} + \text{Da} y \exp(-\mu y)} \quad (30)$$

The steady states are the solutions of

$$\frac{1}{\text{Pe}_\perp^m} \nabla^2 c + (1-c) - N_c [\text{Da}_1 c(1-x-y) - \text{Da}_{-1} x] = 0 \quad (31)$$

$$\text{Da}_2(1-x-y)^2 - \text{Da}_{-1} y^2 - \mathbb{R}(x, y, 0) = 0 \quad (32)$$

where x satisfies Eq. 30. Steady-state bifurcation diagrams were computed by pseudo-arc length continuation. The transversally uniform steady state (\mathbb{U}) is stable to homogeneous perturbations when the two eigenvalues of the Jacobian

$$\mathbb{L} = \begin{bmatrix} -1 - N_c \left\{ \frac{\partial \mathbb{G}_1}{\partial c} + \frac{\partial \mathbb{G}_1}{\partial x} \frac{\partial x}{\partial c} \right\} & -N_c \left\{ \frac{\partial \mathbb{G}_1}{\partial y} + \frac{\partial \mathbb{G}_1}{\partial x} \frac{\partial x}{\partial y} \right\} \\ \frac{\partial(\mathbb{G}_2 - \mathbb{R})}{\partial x} \frac{\partial x}{\partial c} & \frac{\partial(\mathbb{G}_2 - \mathbb{R})}{\partial y} + \frac{\partial(\mathbb{G}_2 - \mathbb{R})}{\partial x} \frac{\partial x}{\partial y} \end{bmatrix} \quad (33)$$

have a negative real part. Uniform oscillatory solution ($\mathbb{U}\mathbb{O}$) emerge at Hopf bifurcation points (\mathbb{H}) at which the two eigenvalues of Eq. 33 are purely imaginary.

To determine the neutral stability points we subject the uniform state to the following small nonuniform perturbation:

$$\boldsymbol{\omega}_{mn}(\xi, \phi) = \begin{bmatrix} \omega_1 J_m(\mu_{mn} \xi) e^{im\phi} \\ \omega_2 J_m(\mu_{mn} \xi) e^{im\phi} \\ \omega_3 J_m(\mu_{mn} \xi) e^{im\phi} \end{bmatrix} \quad (34)$$

where m and n are the azimuthal and radial mode numbers and $e^{im\phi}$ and $J_m(\mu_{mn} \xi)$ are the corresponding eigenfunctions. Because of the no-flux boundary condition at $\xi = 1$, μ_{mn} satisfies the condition

$$\left. \frac{dJ_m(\mu_{mn} \xi)}{d\xi} \right|_{\xi=1} = mJ_m(\mu_{mn}) - \mu_{mn} J_{m+1}(\mu_{mn}) = 0 \quad (35)$$

Table 1. First Nine Eigenvalues Satisfying Eq. 35

No.	m	n	μ_{mn}
1	1	1	1.8412
2	2	1	3.0542
3	0	1	3.8317
4	3	1	4.2012
5	4	1	5.3176
6	1	2	5.3314
7	5	1	6.4156
8	2	2	6.7061
9	0	2	7.0155

The first nine eigenvalues μ_{mn} of the spatial perturbations are reported in Table 1. Only perturbations with $m = 0$ are azimuthally symmetric. An oscillatory neutral stability point is obtained by a simultaneous solution of the steady-state Eqs. 10, 11, and 17 and the associated eigenvalue problem [evaluated around the base state $\boldsymbol{u}_{ss} = (x, y, c, 0)_{ss}$]:

$$-\left(\text{Da}_1 c + \text{Da}_{-1} + \frac{\partial \mathbb{R}}{\partial x} \right) \Big|_{\boldsymbol{u}_{ss}} \omega_1 - \left(\text{Da}_1 c + \frac{\partial \mathbb{R}}{\partial y} \right) \Big|_{\boldsymbol{u}_{ss}} \omega_2 + \text{Da}_1(1-x-y) \Big|_{\boldsymbol{u}_{ss}} \omega_3 = \pm i\sigma \omega_1 \quad (36)$$

$$-\left(2\text{Da}_2(1-x-y) + \frac{\partial \mathbb{R}}{\partial x} \right) \Big|_{\boldsymbol{u}_{ss}} \omega_1 - \left(2\text{Da}_2(1-x-y) + 2\text{Da}_{-2} y + \frac{\partial \mathbb{R}}{\partial y} \right) \Big|_{\boldsymbol{u}_{ss}} \omega_2 = \pm i\sigma \omega_2 \quad (37)$$

$$N_c(\text{Da}_1 c + \text{Da}_{-1}) \Big|_{\boldsymbol{u}_{ss}} \omega_1 + N_c(\text{Da}_1 c) \Big|_{\boldsymbol{u}_{ss}} \omega_2 - \left(\frac{\mu_{mn}^2}{\text{Pe}_\perp^m} + 1 + N_c \text{Da}_1(1-x-y) \right) \Big|_{\boldsymbol{u}_{ss}} \omega_3 = \pm i\sigma \omega_3 \quad (38)$$

where σ is the frequency (up to first-order terms) of the emerging oscillations. [Note that $(\omega_1, \omega_2, \omega_3)$ are complex.] Nonuniform states next to the neutral stability boundary were computed using Eq. 27 as the initial condition.

The eigenvalue Eq. 35 has an infinite number of solutions corresponding to an infinite number of transversal perturbations (Eq. 20), leading to a large number of different types of spatiotemporal patterns. We limit the description and analysis here to spatiotemporal patterns arising from the first three transversal perturbations for $R/d_p = 100$.

Figure 1 shows a case in which a branch of stable, uniform oscillatory states ($\mathbb{U}\mathbb{O}$) exists between two supercritical Hopf points that are on the low limiting-reactant concentration (high conversion) branch of the uniform solutions (\mathbb{U}). (The uniform stationary steady-state solutions bounded between these two supercritical Hopf points are unstable to uniform perturbations.) The corresponding neutral stability points in this case for the first three spatiotemporal patterns: traveling wave ($\mathbb{T}\mathbb{W}$, $\mu_{11} = 1.8412$), antiphase motion ($\mathbb{A}\mathbb{P}$, $\mu_{21} = 3.0542$), and targets (\mathbb{T} , $\mu_{01} = 3.8317$) are very close to the Hopf bifurcation points. Thus, the distinction between these points cannot be shown in the figure. Dynamic simulations close to these neutral stability points, using the initial conditions defined by Eq. 27,

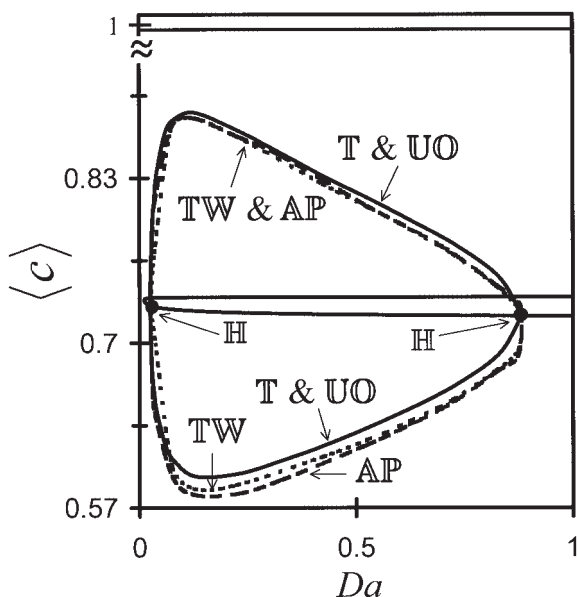


Figure 1. Branches of $\langle c \rangle$ vs. Da plane under isothermal conditions of the uniform steady states (U), and the maxima and minima amplitudes of the uniform oscillatory states (UO), traveling waves (TW), antiphase (AP), and targets (T) motions.

generated traveling waves, antiphase oscillations, and targets. Additional dynamic simulations for various Da were used to determine the branches of the three spatiotemporal states. Figure 1 shows the maximum and minimum of the effluent reactant concentration of these spatiotemporal states and of the uniform oscillatory state. The effluent reactant concentration ($\langle c \rangle$) of the targets and uniform oscillatory states are indistinguishable in this figure. They are slightly higher (lower average conversion) than those of the traveling wave and antiphase motions.

Numerical simulations have shown that the period of the transversal spatiotemporal motions is rather long and close to that of the uniform oscillations. Figure 2a shows that the period (P_{UO}) of the uniform oscillations is of the order of several thousands over a range of Da values. Because the dimensionless time is scaled with respect to the reactor residence time τ_r , the corresponding physical period of the oscillations is

$$t_p = P_{UO}\tau_r \quad (39)$$

Thus, the period of the oscillations is of the order of 2 h for a reactor having a residence time of about 1 s. Figure 2b shows that the percentage deviation between the period of the three spatiotemporal states and that of the uniform oscillations:

$$\% \Delta P = 100 \times (P - P_{UO})/P_{UO} \quad (40)$$

is always small ($< \pm 8\%$).

The simulations indicate that features of the transversal patterns had a minor impact on the temporal effluent reactant

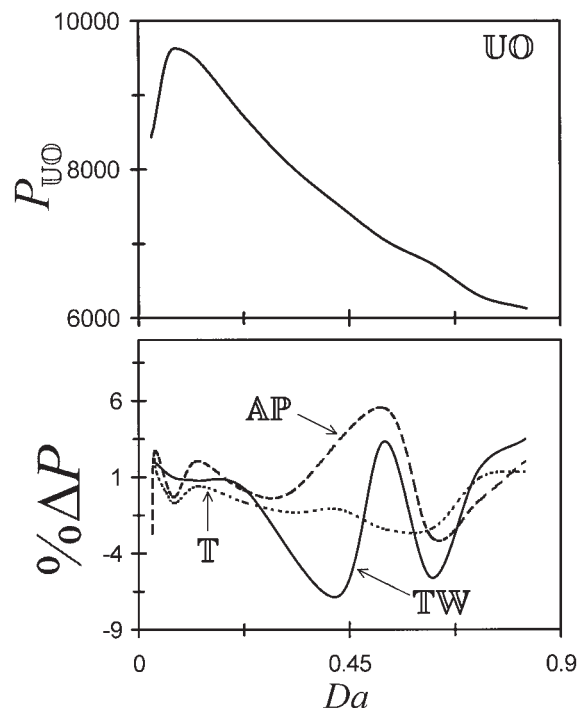


Figure 2. (a) Dependency of the period of uniform oscillatory states on Da . (b) Percentage deviation of the period of the traveling waves (TW), antiphase (AP), and targets (T) motions from that of the uniform oscillatory states.

concentration. Figures 3a and 3b show that the temporal effluent reactant concentration $\langle c \rangle$ of the three patterns (at $Da = 0.224$) oscillated with a rather long period. The temporal ef-

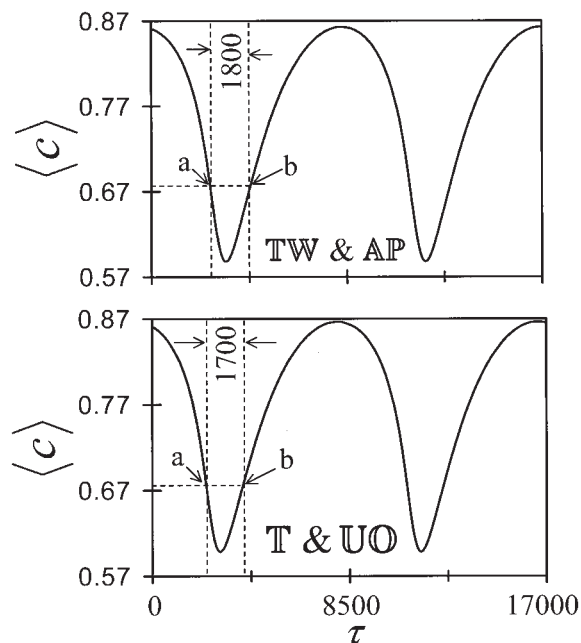


Figure 3. Temporal effluent reactant concentration $\langle c \rangle$ during traveling waves (TW), antiphase (AP), targets (T), and uniform oscillations (UO) at $Da = 0.224$.

fluent reactant concentrations are very close to each other in this example, when either traveling waves or antiphase oscillations occur. Thus, it is not possible to distinguish between them in Figure 3a. Similarly, the temporal effluent concentrations during uniform oscillations or targets motion are very close to each other (Figure 3b). The period of the uniform oscillations and the target pattern is slightly shorter and their temporal effluent reactant concentration differs slightly from that of the other two. The period-averaged effluent reactant concentration in this case is 0.769, 0.77, and 0.773 for the traveling wave, the antiphase motion, and the target motion, respectively. This value is comparable to 0.776 obtained during the uniform oscillations. The effluent reactant concentration of the corresponding unstable (uniform) state is 0.72.

Contour snapshots of the spatial concentration patterns are shown in Figure 4 at two instances for the three transversal patterns. The snapshot, denoted as “a” in Figures 3 and 4, was taken while the temporal effluent concentration is decreasing and the second (“b”) while it was increasing. When a traveling wave (band pattern) exists, a high surface coverage pulse forms near the boundary of the cross section during the period in which the effluent temporal concentration decreases. It travels across the reactor until it reaches a diametrically opposite point on the reactor boundary. The high surface coverage pulse eventually captures the whole cross section. This is followed by the formation of a low surface coverage wave that eventually conquers the surface during the second half of the period. During the antiphase oscillations, two high and low surface coverage zones exist at diametrically opposite locations. The high (low) surface coverage zones eventually expand and capture the whole cross section at the peak (bottom) of the cycle. When a target motion exists, rings of high surface coverage emerge near the boundary and travel to the center until they capture the whole cross section. During the second half of the period, low surface coverage rings emerge near the surface and eventually capture the whole cross section.

Transversal Hot Zone Motion in a Uniformly Active Shallow Reactor

The evolution of spatiotemporal transversal states in an isothermal shallow reactor provides very useful guidance into the formation of nonisothermal transversal states in an adiabatic packed-bed reactor. In the nonisothermal reactor simulations we used the same rate expression and kinetic parameters as those in the isothermal case. The analysis and simulations of

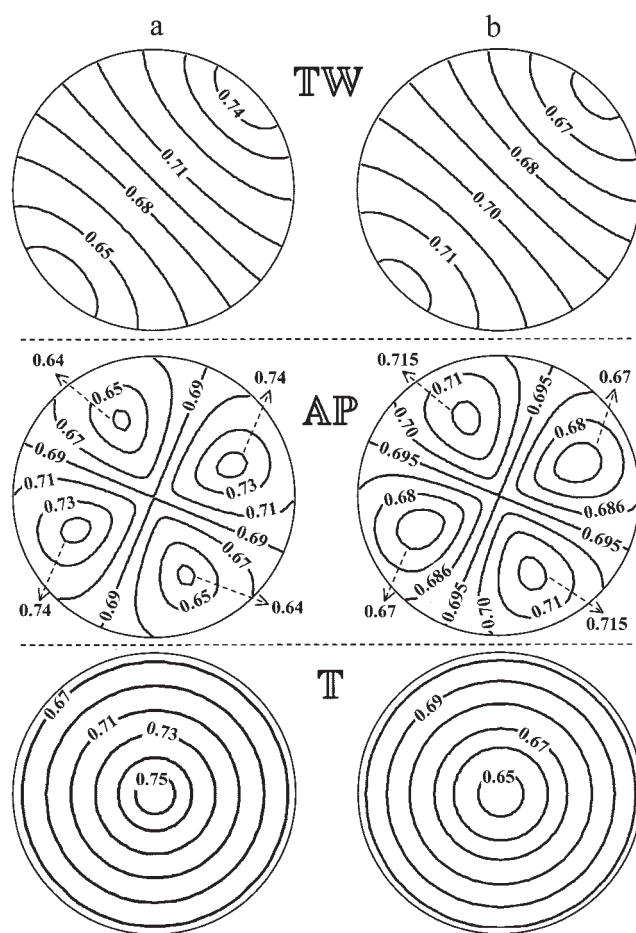


Figure 4. Snapshots of the concentration at two different times (marked as a and b in Figure 3) during traveling waves (TW), antiphase (AP), and targets (T) in an isothermal reactor.

the nonuniform states case are more intricate than those of the isothermal case, but the strategy of finding these states is rather similar. A uniform steady state of the shallow, adiabatic packed-bed reactor is a solution of Eqs. 10 and 11 and Eqs. 16 and 17 after deleting the time derivatives and the terms accounting for the transverse dispersion. A uniform steady state is stable to homogeneous perturbations when all the eigenvalues of the Jacobian

$$\mathbb{L}_N = \begin{bmatrix} \frac{\partial(G_1 - R)}{\partial x} & \frac{\partial(G_1 - R)}{\partial y} & \frac{\partial G_1}{\partial c} & \frac{\partial(G_1 - R)}{\partial \theta} \\ \frac{\partial(G_2 - R)}{\partial x} & \frac{\partial(G_2 - R)}{\partial y} & 0 & \frac{\partial(G_2 - R)}{\partial \theta} \\ \frac{\beta N_c}{Le} \frac{\partial R}{\partial x} & \frac{\beta N_c}{Le} \frac{\partial R}{\partial y} & 0 & \frac{1}{Le} \left(-1 + \beta N_c \frac{\partial R}{\partial \theta} \right) \\ -N_c \frac{\partial G_1}{\partial x} & -N_c \frac{\partial G_1}{\partial y} & -1 - N_c \frac{\partial G_1}{\partial c} & -N_c \frac{\partial G_1}{\partial \theta} \end{bmatrix} \quad (41)$$

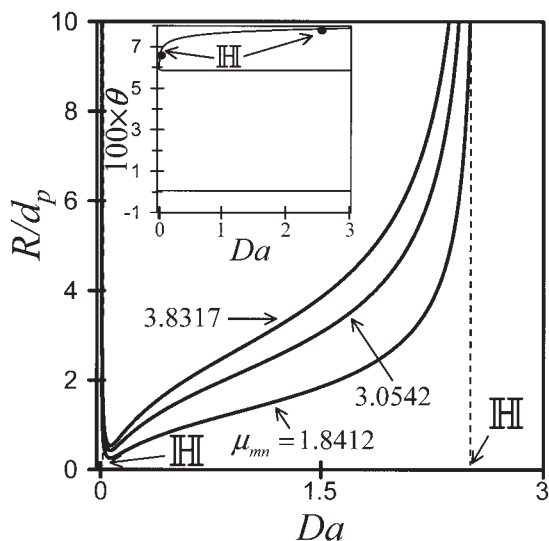


Figure 5. Neutral stability curves for the first three transversal modes in the R/d_p vs. Da plane.

Inset: Branches of uniform steady states in the θ vs. Da plane.

evaluated at $\mathbf{u}_{ss} = (x, y, c, \theta)_{ss}$ have a negative real part. At a Hopf bifurcation, \mathbb{L}_N has a pair of purely imaginary eigenvalues.

To determine a neutral stability point at which a transition to a spatiotemporal state occurs, we expose a uniform unstable steady state, bounded between two Hopf points to small spatial nonuniform perturbations of the form

$$\boldsymbol{\omega}_{mn}(\xi, \phi) = \begin{bmatrix} \omega_1 J_m(\mu_{mn} \xi) e^{im\phi} \\ \omega_2 J_m(\mu_{mn} \xi) e^{im\phi} \\ \omega_3 J_m(\mu_{mn} \xi) e^{im\phi} \\ \omega_4 J_m(\mu_{mn} \xi) e^{im\phi} \end{bmatrix} \quad (42)$$

where J_m is the Bessel function of first kind and μ_{mn} is the transverse spatial eigenvalue that satisfies Eq. 35. The state on the neutral stability point satisfies the steady-state equations and the linearized eigenvalue problem

$$(\mathbb{L}_N - \mathbb{P}) \cdot (\boldsymbol{\omega}_r \pm i\boldsymbol{\omega}_i) = \pm i\sigma(\boldsymbol{\omega}_r \pm i\boldsymbol{\omega}_i) \quad (43)$$

where

$$\mathbb{P} = \begin{bmatrix} 0 & 0 & 0 & 0 \\ 0 & 0 & 0 & 0 \\ 0 & 0 & \mu_{mn}^2 / (\text{Le Pe}_\perp^h) & 0 \\ 0 & 0 & 0 & \mu_{mn}^2 / \text{Pe}_\perp^m \end{bmatrix} \quad (44)$$

The oscillatory neutral stability curves for the first three transverse modes are shown in Figure 5. The bifurcation diagram of the corresponding stationary uniform states is shown in the insert of that figure. Two supercritical Hopf bifurcation points (at which a branch of stable, uniform oscillations emerge) exist on the high-temperature branch of the uniform solutions. Values of σ at the two limiting Hopf points are 5×10^{-4} and 12×10^{-4} , which correspond to an oscillation period ($2\pi/\sigma$) on the order of 5200 and 12,000. A branch of uniform

stable oscillatory states exists between these two supercritical Hopf points. The neutral stability curves are bounded between the Da values of these two Hopf points. These curves asymptotically approach the two Hopf bifurcation points at very large values of R/d_p . The simulations show that the neutral stability curve of any mode is always contained within those of the lower modes.

The spatiotemporal solutions were obtained, as were those in the isothermal case, by perturbing the unstable, uniform high-temperature steady state \mathbf{u}_{ss} close to the neutral stability curve with the transverse spatial modes (Eq. 27). Dynamic simulations were used to determine the branches of these spatiotemporal states. Each mode of perturbation can lead to a different type of spatiotemporal transversal temperature pattern. We restrict the analysis here to the patterns obtained by spatial perturbations corresponding to the first three modes for $R/d_p = 100$.

Figure 6 shows the initial conditions used to generate the three types of spatiotemporal patterns and snapshots of the instantaneous transversal reactor temperature at five instances (marked as a–e on the reactor effluent temperature time series shown in Figure 7). The times at which the snapshots shown in Figure 6 were taken are reported in Table 2. The first mode leads to a *band* pattern (B). In this case, a high-temperature pulse forms near the boundary. A high-temperature band travels across the reactor cross section until it reaches a diametrically opposite point on the reactor boundary and captures the

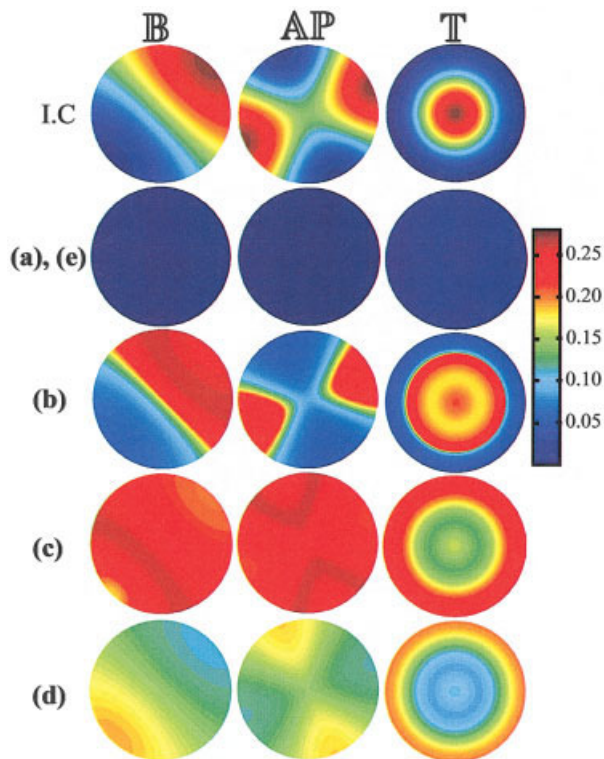


Figure 6. Snapshots of the temperature at times marked as a–e in Figure 7 during band pattern (B), antiphase (AP), and targets (T) motions.

The initial condition leading to these are shown in the first row (marked as I.C.). (Table 2 reports the snapshot times.)

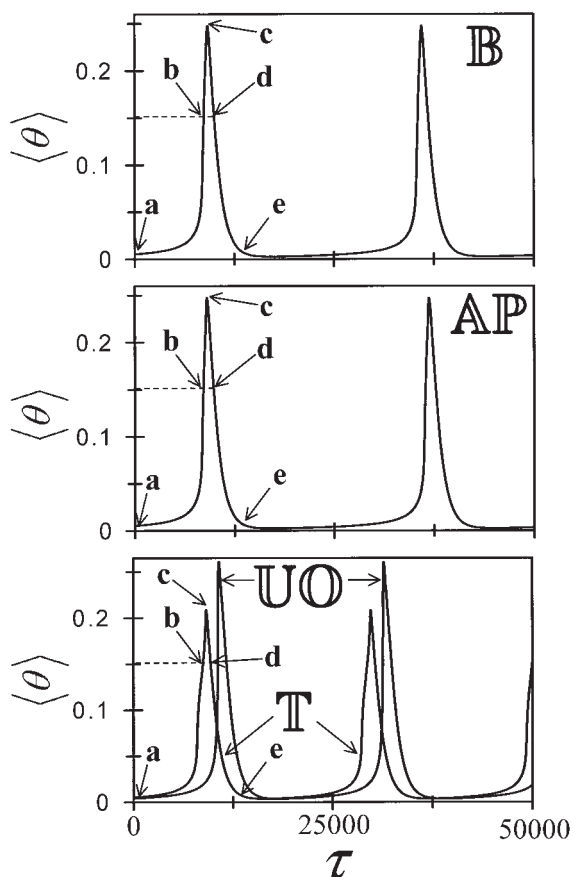


Figure 7. Temporal effluent temperature $\langle \theta \rangle$ during band pattern (B), antiphase (AP), and targets (T) motions at $Da = 0.09$.

whole cross section. During the second part of the period, a low-temperature pulse forms that eventually captures the whole surface. The second mode leads to *antiphase* oscillations (AP). Here, two high-temperature and two low-temperature zones form at diametrically opposite locations. The high-temperature (low-temperature) zones eventually expand and capture the whole cross section at the instant denoted as c (e) in the reactor effluent time series in Figure 7. The third mode generates a target pattern (T). In this case, high-temperature rings emerge near the boundary and travel to the reactor center until they capture the whole cross section. During the second half of the period, low-temperature rings form and eventually capture the whole surface.

The temporal reactor effluent temperatures during the periodic band, antiphase, target motions, and uniform oscillations are shown in Figure 7 for the same set of parameters. The time series of each period of the motions consists of a peak and a quiescent section. The spatiotemporal motion is dominant during the peak in the time series, whereas the reactor temperature is similar to a uniform, extinguished state during the quiescent section of the time series. Temporal temperatures of the band and antiphase motions are very similar. The peak temperature and conversion during the target motion were somewhat lower. Periods of both the band and the antiphase motions are very similar and of the order of 25,000. The period of the target motion is somewhat shorter, of the order of 20,600. The period

of uniform oscillations is about 20,750. Several qualitative features, such as the temporal effluent temperature or reactant concentration, and the features of the spatiotemporal motions obtained during the nonisothermal operation are very similar to those obtained in the isothermal case. The period of the spatiotemporal motions in the nonisothermal case is about three-fold longer than that in the isothermal case.

It is very difficult to identify and determine the dynamic features of the spatiotemporal motions from inspection of the sequence of temporal patterns. This identification can be simplified by using *principal-component analysis* (PCA) to decompose the spatiotemporal patterns into orthogonal time-independent spatial modes (or principal modes) and time-dependent amplitudes.⁴⁷ This procedure provides an objective method for learning about the underlying dynamics in space and time and has been successfully applied to the analysis of spatiotemporal patterns on catalytic surfaces.^{9,48-50} In this procedure, the spatiotemporal data $\mathbf{u}(\xi, \phi, \tau)$ are represented by the series

$$\mathbf{u}(\xi, \phi, \tau) = \sum_{i=1}^N \mathcal{A}_i(\tau) \varphi_i(\xi, \phi) \quad (46)$$

where $\mathcal{A}_i(\tau)$ represents orthogonal time-dependent amplitudes and $\varphi_i(\xi, \phi)$ represents spatial modes. Thus,

$$\langle \varphi_i(\xi, \phi) \cdot \varphi_j(\xi, \phi) \rangle = \delta_{ij} \quad (47)$$

$$\overline{\mathcal{A}_i(\tau) \mathcal{A}_j(\tau)} = \lambda_i \delta_{ij} \quad (48)$$

The $\varphi_i(\xi, \phi)$ values are determined from s snapshots of the temporal patterns; specifically these modes are the eigenvectors of the eigenvalue problem

$$\mathbb{A} \varphi_i(\xi, \phi) = \lambda_i \varphi_i(\xi, \phi) \quad (49)$$

where the autocorrelation matrix

$$\mathbb{A} = \frac{1}{s} \sum_{i=1}^s \mathbf{u}(\xi, \phi, \tau_i) \mathbf{u}[(\xi, \phi)', \tau_i] \quad (50)$$

and λ_i reflects the energy corresponding to a particular spatial mode $\varphi_i(\xi, \phi)$, that is, the fractional contribution of a specific mode to the dynamics of the pattern. The amplitudes $\mathcal{A}_i(\tau)$ are the projections of the data set $\mathbf{u}(\xi, \phi, \tau)$ on $\varphi_i(\xi, \phi)$, that is,

Table 2. Times at Which the Snapshots Shown in Figure 6 Were Taken

	B	AP	T
a	0	0	0
b	8607	8598	8728
c	9169	9080	9193
d	9962	9867	9704
e	14,090	13,665	13,721

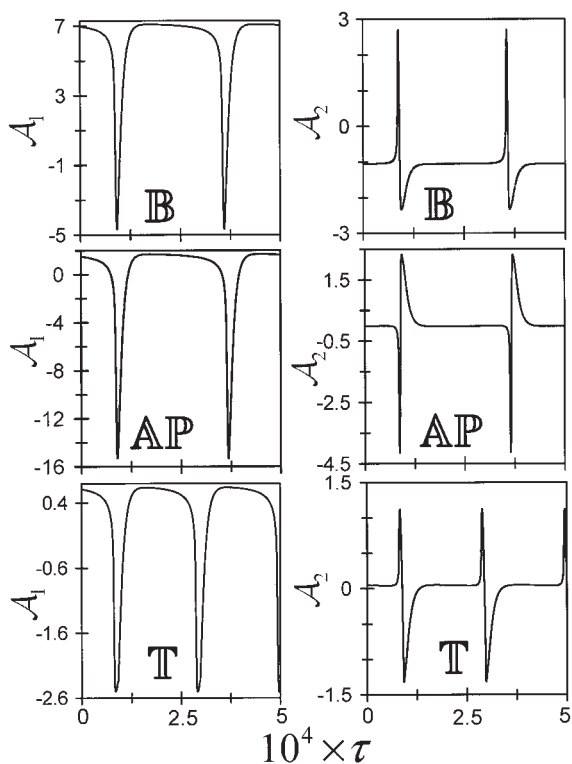


Figure 8. Temporal amplitudes of the first two principal modes of the PCA for band pattern (B), antiphase (AP), and targets (T).

$$\mathcal{A}_i(\tau) = \sum_{i=1}^s \mathbf{u}(\xi, \phi, \tau_i) \varphi_i(\xi, \phi) \quad (51)$$

The principal component analysis routine in Matlab[®] 51 was used to conduct this analysis.

The first two principal modes of all three motions captured more than 95% of the energy associated with the pattern. Thus, we present in Figure 8 only the temporal amplitudes of these two principal modes. The two principal modes had the same period of oscillation, that is, had the same oscillation frequency. The temporal amplitudes capture the main feature of the time series shown in Figure 7—the existence of a peak followed by a quiescent period.

The contours of the first two PCA modes and the corresponding phase plot of their amplitudes for the three patterns are shown in Figure 9. (We placed a black rim at the circumference of the PCA mode contours to mark its area.) They are of the motions described in Figures 6 and 7. The two principal modes of the band pattern, shown in Figure 9, have the qualitative features of the first transversal mode. Similarly, the two principal modes of the antiphase motion have the same features as those of the second transversal mode. The two modes are $\pi/2$ rotation of each other. The first principal mode of the targets has three zones: high (hot), low (cold), and high (hot) in that order starting from the center ($\xi = 0$) of the reactor. This spatial profile is similar to the ninth transversal mode. The second principal mode has two zones, high (hot) and low (cold), which is similar to the third transversal mode.

The marks of “a” to “e” on the phase plots in Figure 9 correspond to the marked states in Figure 7. Inspecting these points indicates the relative contribution from the first two modes to the temperature snapshots in Figure 6. The amplitudes of the first two modes remained unchanged for a long time at the sharp tip on the phase plot (H). This tip point corresponds to the long quiescent period during which the reactor remains at an extinguished state. The rich spatiotemporal dynamics during the peak in Figure 7 is reflected by the looping of the amplitudes in the phase plot. This fast looping followed by a long sojourn next to a point on the phase plot is a typical behavior of a homoclinic cycle.^{52,53} Although the temporal snapshots of the three motions are qualitatively very different, they all exhibit homoclinic motion. The homoclinic nature of these motions is responsible for the rather long period of oscillation. This predicted feature was observed experimentally during CO oxidation.⁹

Discussion and Conclusions

Previous studies were able to predict stationary hot zone formation in a packed-bed reactor only by making the unrealistic assumption that the transversal heat dispersion in the reactor is smaller than that of the limiting reactant. Viswanathan et al.²⁴ proved that a pseudo-homogeneous model of a shallow adiabatic packed-bed reactor cannot predict a

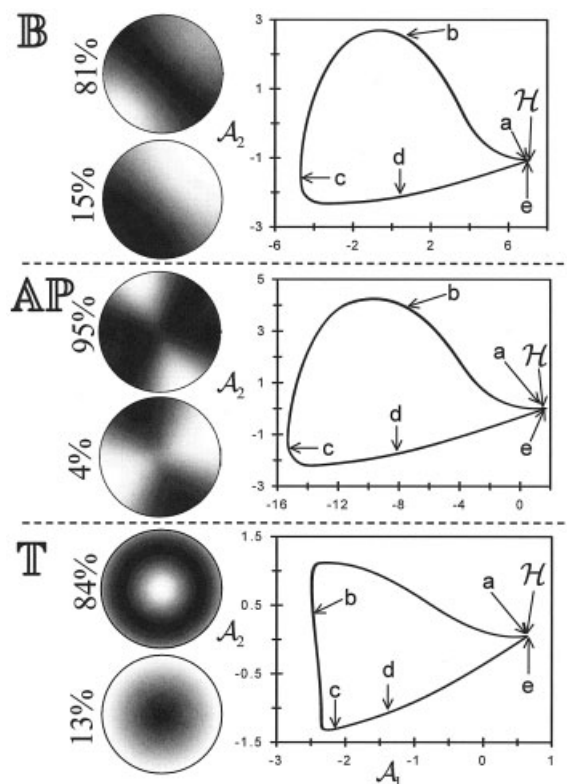


Figure 9. First two principal modes of the PCA and the phase plane of the corresponding temporal amplitudes for band pattern (B), antiphase (AP), and targets (T).

Points a–e correspond to those in Figure 7. White = high, black = low.

bifurcation to a stable stationary, transversal, nonuniform state under the practical condition that the transversal heat dispersion in the reactor exceeds that of the limiting reactant. This conclusion was proven for reactions whose rate depends only on the surface concentration of the limiting reactant and temperature. Our study shows that the reaction kinetics has a major influence on whether stable, transversal, spatiotemporal hot zones can be predicted to exist in a uniformly active shallow packed-bed reactor under the realistic condition that the transversal heat dispersion in the reactor exceeds that of the limiting reactant. This insight is of both fundamental and practical importance and is an important step toward gaining an understanding of the formation of transversal hot zones in packed-bed reactors.

Our simulations and analyses are for a catalytic reaction, the rate of which may exhibit isothermal rate oscillations. Several mechanisms and rate expressions proposed in the literature can predict such a behavior.²⁶⁻³⁶ Ertl's research group²⁶ proved that this type of oscillations may occur during ultralow-pressure CO oxidation. All these rate expressions are more detailed and intricate than those used in traditional reactor design models. We use in this study one of these rate expressions. Our success in finding the spatiotemporal states hinged on our ability to predict the neutral stability curve and the corresponding modes. Without this knowledge, the simulations tend to lead to the uniform oscillatory states. The prediction of the transversal hot zones requires knowledge of the detailed reaction rate expression. Our study suggests that prediction of the hot spots may require models that are more detailed than those used in the reactor design. An important intriguing question is what other reaction rate expressions and reaction networks can generate transversal hot zones.

Our study indicates that essentially a very large number of different patterns may be generated for a sufficiently large reactor diameter. Each of these states has a rather limited region of attraction. It is highly conceivable that when many different stable, spatiotemporal states can form for a specific set of parameters, small perturbations will cause a shift from one to the other. This may lead to formation of a chaotic attractor with a region of attraction larger than that of the individual states.

One of the surprising findings of experimental studies in shallow packed-bed reactors is the rather long period of the oscillations (order of hours).^{9,10} The homoclinic nature of the motion, revealed by the PCA of our simulations, is responsible for this unexpected long period, which has also been observed experimentally. The rather slow oscillations in the isothermal case indicate that the reaction kinetics—and not the thermal dispersion time constant—is the main reason for the long period of oscillations. This finding differs from what has been previously assumed.

The qualitative features of the three motions are rather different. Yet, the period of their motions and the corresponding reactant effluent concentrations were very close to each other and to those of the uniform oscillatory state. This is a rather surprising finding for which we have not yet found an answer.

Acknowledgments

We gratefully acknowledge the support of this research by grants from the National Science Foundation and the Welch Foundation. Computations

were performed at the San Diego Supercomputing Center. We are most grateful to Dr. Andrew Salinger, Prof. Martin Golubitsky, and Prof. Geminu Gunaratne for very helpful discussions and advice.

Notation

a_v	= catalyst-specific surface area, m^2_{surf}/m^3
A	= constant coefficient for initial conditions in Eq. 27
\mathcal{A}	= amplitudes of the principal modes
\mathbb{A}	= autocorrelation matrix, defined by Eq. 50
AP	= antiphase
c	= dimensionless concentration, defined by Eq. 5
C	= concentration, mol/m^3
C_p	= specific heat capacity, $\text{J kg}^{-1} \text{K}^{-1}$
d_p	= particle diameter, m
D	= species diffusion coefficient, m^2/s
Da	= Damköhler number, defined by Eq. 15
$\mathbb{D}_v \mathbb{F}$	= first Fréchet derivative
E	= activation energy, J/mol
\mathbb{F}	= vector of steady-state equations
\mathbb{G}_1	= dimensionless rate of adsorption of A , defined by Eq. 12
\mathbb{G}_2	= dimensionless rate of adsorption of B , defined by Eq. 14
h	= interfacial heat transfer coefficient, $\text{W K}^{-1} m^{-2}$
\mathbb{H}	= Hopf bifurcation
J	= Bessel function of first kind
k	= adsorption or reaction rate constant
L	= length of the reactor, m
\mathbb{L}	= linearized matrix
Le	= Lewis number, defined by Eq. 5
M	= adsorption capacity, $\text{mol}/m^2_{\text{surf}}$
N	= radial grid points
N_c	= dimensionless adsorption capacity, defined by Eq. 5
P	= period of oscillations
\mathbb{P}	= transversal perturbation matrix
Pe	= Peclet number, defined by Eq. 5
r	= radial coordinate, m
R	= radius of the reactor, m
\bar{R}	= universal gas constant, $\text{J mol}^{-1} \text{K}^{-1}$
\mathbb{R}	= dimensionless reaction rate, defined by Eq. 13
s	= number of snapshots
t	= time, s
t_p	= period of oscillations, s
T	= temperature, K
\mathbb{T}	= targets
TW	= traveling wave
\mathbf{u}	= vector of state variables
\mathbb{U}	= uniform stationary
\mathbb{UO}	= uniform oscillatory
v	= superficial fluid velocity, m/s
x	= fractional surface coverage of species A
y	= fractional surface coverage of species B
z	= axial coordinate, m

Greek letters

β	= adiabatic temperature rise, defined by Eq. 5
γ	= dimensionless activation energy, defined by Eq. 15
δ	= Kronecker delta function
ε	= bed voidage
η	= dimension axial coordinate, defined by Eq. 5
θ	= dimensionless temperature, defined by Eq. 5
$\bar{\lambda}$	= effective thermal conductivity, $\text{W m}^{-1} \text{K}^{-1}$
λ_{sg}	= thermal conductivity, $\text{W m}^{-1} \text{K}^{-1}$
λ	= eigenvalue of autocorrelation matrix
μ	= surface coverage factor
μ_{mn}	= transversal eigenmodes
ξ	= dimensionless radial coordinate, defined by Eq. 5
ρ	= density, kg/m^3
σ	= coefficient of imaginary eigenvalue
τ	= dimensionless time, defined by Eq. 5
τ_r	= residence time, s
φ	= principal mode
ϕ	= azimuthal coordinate
ψ	= eigenvector of principal component analysis

- ω = eigenvector
- ω_{mn} = transversal perturbation vector, defined by Eq. 20
- $-\Delta H$ = heat of the reaction, J/mol
- ΔP = percentage period change, defined by Eq. 40
- Ψ = matrix of eigenvectors ψ

Others

- ∇^2 = Laplacian in polar coordinates
- $\langle \cdot \rangle$ = spatially averaged quantity

Superscripts

- h = heat
- m = mass

Subscripts

- a = axial
- A = species A
- B = species B
- g = gas phase
- i = imaginary
- in = inlet
- m = azimuthal mode number
- n = radial mode number
- N = nonisothermal
- r = real
- s = solid
- ss = steady state
- \perp = transversal

Literature Cited

1. Borekov GK, Matros YuSh, Klenov OP, Logovkoi VI, Lakhmostov VS. Local nonuniformities in a catalyst bed. *Dokl Akad Nauk SSSR*. 1981;258:1418-1420.
2. Matros YS. *Unsteady Processes in Catalytic Reactors*. Amsterdam: Elsevier; 1985.
3. Barkelew CH, Gambhir BS. Stability of trickle-bed reactors. *ACS Symp Ser*. 1984;237:61-81.
4. Wicke E, Onken HU. Periodicity and chaos in a catalytic packed bed reactor for CO oxidation. *Chem Eng Sci*. 1988;43:2289-2294.
5. Wicke E, Onken HU. Bifurcation, periodicity and chaos by thermal effects in heterogeneous catalysis. In: Markus M, Muller SC, Nicolis G, eds. *From Chemical to Biological Organization*. Berlin/New York: Springer-Verlag; 1988:68-81.
6. Marwaha B, Annamalai J, Luss D. Hot zone formation during carbon monoxide oxidation in a radial flow reactor. *Chem Eng Sci*. 2001;56:89-96.
7. Marwaha B, Luss D. Formation and dynamics of a hot zone in radial flow reactor. *AIChE J*. 2002;48:617-624.
8. Marwaha B, Luss D. Hot zone formation in packed bed reactors. *Chem Eng Sci*. 2003;58:733-738.
9. Marwaha B, Sundarram S, Luss D. Dynamics of transversal hot zones in shallow packed bed reactors. *J Phys Chem B*. 2004;108:14470-14476.
10. Marwaha B, Sundarram S, Luss D. Dynamics of hot zones on top of packed bed reactors. *Chem Eng Sci*. 2004;59:5569-5574.
11. Digilov R, Nekhamkina O, Sheintuch M. Thermal imaging of breathing patterns during CO oxidation on a Pd/glass cloth. *AIChE J*. 2004;1:163-172.
12. Sundarram S, Marwaha B, Luss D. Global coupling induced temperature patterns on top of packed bed reactors. *Chem Eng Sci*. 2005;60:6803-6805.
13. Jaffe SB. Hot spot simulation in commercial hydrogenation processes. *Ind Eng Chem Process Des Dev*. 1976;15:410-416.
14. Stroh F, Balakotaiah V. Modeling of reaction induced flow maldistributions in packed-beds. *AIChE J*. 1991;37:1035-1052.
15. Nguyen D, Balakotaiah V. Flow maldistributions and hot spots in down-flow packed bed reactors. *Chem Eng Sci*. 1994;49:5489-5505.
16. Nguyen D, Balakotaiah V. Reaction-driven instabilities in down-flow packed beds. *Proc R Soc Lond A Phys Sci*. 1995;450:1-21.
17. Subramanian S, Balakotaiah V. Analysis and classification of reaction driven stationary convective patterns in a porous medium. *Phys Fluids*. 1997;9:1674-1695.
18. Benneker AH, Kronberg AE, Westerterp KR. Influence of buoyancy forces on the flow of gases through packed beds at elevated pressures. *AIChE J*. 1998;44:263-270.
19. Middya U, Luss D, Sheintuch M. Spatiotemporal motions due to global interaction. *J Chem Phys*. 1994;100:3568-3581.
20. Nekhamkina O, Digilov R, Sheintuch M. Modeling of temporally-complex breathing patterns during Pd-catalyzed CO oxidation. *J Chem Phys*. 2002;119:2322-2332.
21. Schmitz RA, Tsotsis TT. Spatially patterned states in systems of interacting catalyst particles. *Chem Eng Sci*. 1983;38:1431-1437.
22. Balakotaiah V, Christaforatou EL, West DH. Transverse concentration and temperature non-uniformities in adiabatic packed bed catalytic reactors. *Chem Eng Sci*. 1999;54:1725-1734.
23. Yakhin V, Menzinger M. On transverse patterns in catalytic packed bed reactors. *Chem Eng Sci*. 2001;56:2233-2236.
24. Viswanathan G, Bindal A, Khinast J, Luss D. Stationary transversal hot zones in adiabatic packed bed reactors. *AIChE J*. 2005;51. in press.
25. Asakura K, Lauterbach J, Rotermund HH, Ertl G. Spatiotemporal concentration patterns associated with the catalytic oxidation of CO on Au covered Pt(110) surfaces. *J Chem Phys*. 1995;102:8175-8184.
26. Krischer K, Eiswirth M, Ertl G. Oscillatory CO oxidation on Pt(110): Modeling of temporal self-organization. *J Chem Phys*. 1992;96:9161-9172.
27. Imbihl R, Ertl G. Oscillatory kinetics in heterogeneous catalysis. *Chem Rev*. 1995;95:697-733.
28. Belyaev VD, Slinko MM, Slinko MG. Self-oscillations in the catalytic rate of heterogeneous hydrogen oxidation on nickel and platinum. In: Bond GC, Wells PB, Tompkins FC, eds. *Proceedings of the Sixth International Congress on Catalysis*. Vol. 2. London, UK: The Chemical Society; 1976:758-767.
29. Slinko MG, Slinko MM. Self-oscillations of heterogeneous catalytic reaction rates. *Catal Rev Sci Eng*. 1978;17:119-153.
30. Ivanov EA, Chumakov GA, Slinko MG, Bruns DD, Luss D. Isothermal sustained oscillations due to the influence of adsorbed species on the catalytic reaction rate. *Chem Eng Sci*. 1980;35:795-803.
31. Sales BC, Turner JE, Maple MB. Oscillatory oxidation of CO over a Pt catalyst. *Surf Sci*. 1981;103:54-74.
32. Slinko MM, Kurkina ES, Liauw MA, Jaeger NI. Mathematical modeling of complex oscillatory phenomena during CO oxidation over Pd zeolite catalysts. *J Chem Phys*. 1999;17:8105-8114.
33. Eigenberger G. Kinetic instabilities in heterogeneously catalyzed reactions—1. Rate multiplicity with Langmuir-type kinetics. *Chem Eng Sci*. 1978;33:1255-1261.
34. Eigenberger G. Kinetic instabilities in heterogeneously catalyzed reactions—2. Oscillatory instabilities with Langmuir-type kinetics. *Chem Eng Sci*. 1978;33:1263-1268.
35. Collins NA, Sundaresan S, Chabal YJ. Studies on self-sustained reaction-rate oscillations. III. The carbon model. *Surf Sci*. 1987;180:136-152.
36. Wicke E, Kummann P, Keil W, Schiefeler J. Unstable and oscillatory behavior in heterogeneous catalysis. *Ber Bunsenges Phys Chem*. 1980;84:315-323.
37. Vortmeyer D, Schaeffer RJ. Equivalence of one- and two-phase models for heat transfer processes in packed beds: One dimensional theory. *Chem Eng Sci*. 1974;29:485-491.
38. Peskov NV, Slinko MM, Jaeger NI. Mathematical model of reaction rate oscillations on a chain of nm-sized catalyst particles. *J Chem Phys*. 2003;118:8882-8890.
39. Golubitsky M, Schaeffer DG. *Singularities and Groups in Bifurcation Theory*. Vol. I. New York, NY: Springer-Verlag; 1984.
40. Balakotaiah V, Gupta N, West DH. Transport limited pattern formation in catalytic monoliths. *Chem Eng Sci*. 2002;57:435-448.
41. Viswanathan GA. *Transversal Temperature Patterns in Packed Bed Reactors*. PhD Dissertation. Houston, TX: University of Houston; 2004.
42. Middya U, Luss D. Impact of global interaction on pattern formation on a disk. *J Chem Phys*. 1995;102:5029-5036.
43. Deuffhard P, Hairer E, Zueck J. One-step extrapolation methods for differential-algebraic systems. *J Numer Math*. 1987;51:501-516.
44. Ehrig R, Nowak U, Oeverdieck L, Deuffhard P. Advanced extrapolations methods for large scale differential algebraic problems. In: Bun-

- gartz H-J, Durst F, Zenger Chr, eds. *High Performance Scientific and Engineering Computing* (Lecture Notes in Computational Science and Engineering). Vol. 8. Munich: Springer-Verlag; 1999:233-244.
45. Golubitsky M, Stewart I, Knobloch E. Target patterns and spirals in planar reaction-diffusion systems. *J Nonlinear Sci.* 2000;10:333-354.
46. Slinko MM, Jaeger NI. Oscillating heterogeneous catalytic systems. *Studies in Surface Science and Catalysis*. Vol. 86. Amsterdam, The Netherlands: Elsevier; 1994.
47. Palacios A, Gunaratne GH, Gorman M, Robbins KA. Karhunen-Loève analysis of spatiotemporal flame patterns. *Phys Rev E.* 1998; 57:5958-5971.
48. Graham MD, Lane SL, Luss D. Proper orthogonal decomposition analysis of spatiotemporal temperature patterns. *J Phys Chem.* 1993; 97:889-894.
49. Chen C-C, Wolf EE, Chang H-C. Low-dimensional spatiotemporal thermal dynamics on nonuniform catalytic surfaces. *J Phys Chem.* 1993;97:1055-1064.
50. Krischer K, Rico-Martinez R, Kevrekidis IG, Rotermund HH, Ertl G. Model identification of a spatiotemporally varying catalytic reaction. *AIChE J.* 1993;39:89-98.
51. The MathWorks. *Statistics Toolbox For Use with Matlab®—User's Guide*, Ver. 5.0.2. (http://www.mathworks.com/access/helpdesk/help/pdf_doc/stats/stats.pdf). Natick, MA: The MathWorks Inc.; 2005.
52. Guckenheimer J, Holmes P. *Nonlinear Oscillations, Dynamical Systems and Bifurcations of Vector Fields*. New York, NY: Springer-Verlag; 1983.
53. Golubitsky M, Stewart I, Schaeffer DG. *Singularities and Groups in Bifurcation Theory*. Vol. II. New York, NY: Springer-Verlag; 1988.

Manuscript received Apr. 24, 2005, and revision received Jun. 25, 2005.